CrossMark

Fracture behavior of a composite composed by Ti-aluminide multi-layered and continuous-SiC$_f$-reinforced Ti-matrix

Kai Zhu, Yan-Jin Xu* , **Tao Jing, Hong-Liang Hou**

Abstract In the present work, a novel hybrid composite composed of Ti-aluminide multi-layered part and continuous-SiC$_f$-reinforced Ti-matrix part using a vacuum hot pressing/hot isostatic pressure (VHP/HIP) sintering process was synthesized. Then, the damage tolerance behavior of this hybrid composite was studied by tensile tests and in situ scanning electron microscopy (SEM) three-point bending tests. The results indicate that the mechanical properties and crack propagation of the hybrid composite are strongly influenced by the extrinsic toughness mechanism. In detail, the crack deflection of multi-layered composite and strengthening effect of SiC$_f$-reinforced matrix composite are observed in the hybrid composite. Owing to the strengthening effect of continuous-SiC$_f$-reinforced Ti-matrix part, the tensile strength of hybrid composite is much higher than that of neat Ti-aluminide multi-layered composite. Furthermore, it is found that the optimal damage tolerance ability is optimized when the notch position is located at the Ti-aluminide multi-layered part due to the crack deflection of multi-layered structure.

Keywords Hybrid composite; Synthesis; Mechanical properties; In situ observation

K. Zhu, T. Jing
School of Materials Science and Engineering, Tsinghua University, Beijing 100084, China

Y.-J. Xu*, H.-L. Hou
Metal Forming Technology Department, Beijing Aeronautical Manufacturing Technology Research Institute, Beijing 100024, China
e-mail: xuyj_avic@qq.com

1 Introduction

During the last years, various metal–intermetallic multi-layered materials have been fabricated and investigated due to their attractive mechanical properties such as high specific strength, high specific stiffness and high toughness [1–4]. Subsequently, huge studies have been done to characterize their damage tolerance in order to ensure their reliabilities in structural applications [5–8]. The extrinsic toughening mechanisms, including crack deflection, crack blunting and crack bridging, are traceable to the alternatively arranged brittle layers and ductile layers. This arrangement enhances the fracture toughness and energy absorption abilities of these composites [9–11]. Among these metal–intermetallic multi-layered materials, Ti-aluminide multi-layered composite is considered as one of the most promising engineering materials due to the relative low density and high elevated temperature strength. However, the Ti–Al compounds in multi-layered composite are brittle at room temperature, which severely decreases the tensile strength of the Ti-aluminide multi-layered composites and hinder their applications [12, 13]. Aiming to overcome this shortcoming and optimize the mechanical properties of the Ti-aluminide multi-layered composite, a continuous-SiC$_f$-reinforced Ti-matrix part was successfully sintered on the Ti-aluminide multi-layered part in this work. According to previous research results, continuous-SiC$_f$-reinforced Ti-matrix possesses excellent mechanical properties due to the reinforcement effect of the fibers [12, 14, 15]. More importantly, it was reported that the fragment of SiC fibers could still reinforce the Ti-matrix as particles during three-point bending test [12, 16, 17].

Therefore, the objective of this work is to fabricate this new type of hybrid composite possessing high tensile strength and good fracture resistance by integrating the Ti-aluminide multi-layered composite and the continuous-SiC_f-reinforced titanium composite to form a hybrid material. The vacuum hot press (VHP) method [18, 19] was used to fabricate the novel hybrid composite. Hot isostatic- pressure (HIP) was applied to densify this composite and eliminate the internal voids. Finally, in situ scanning electron microscopy (SEM) observation was used to characterize the damage tolerance behavior of this novel composite during three-point bending test. For comparison, the neat Ti-aluminide multi-layered composite was also produced.

2 Experimental

2.1 Preform preparation and sintering procedure for hybrid composite manufacture

The elemental materials used in this study were commercial pure Ti foils (>99%), pure Al foils (>99%) and continuous SiC fibers (Beijing Institute of Aeronautical Materials, China). The thicknesses of the Ti foils and Al foils were 100 and 40 μm, respectively. All the foils were cut into square sheets with the dimension of 35 mm × 35 mm for later use. Noticeably, the initially selected thickness ratio of 5:2 is to make sure that all the Al foils can be consumed into Ti–Al compounds after the whole sintering process. The detailed preprocessing method of the three elemental components has already been presented elsewhere [20]. After all the pretreatment processes, the Ti foils, Al foils and SiC fiber tapes were stacked and bound together, as presented in Fig. 1. Here, it should be noted that all the SiC fiber tapes were aligned in the same direction.

After the stacking stage, the precursor was carefully moved into a vacuum hot press furnace. Then, for the purpose of eliminating the porosities and defects, HIP was

applied. Figure 2 presents the combined VHP/HIP configuration and processing parameters of the fabrication process.

2.2 Materials characterization

For the microstructural observation, the specimens were sectioned from the novel hybrid composite by the electro-discharge machining. After that, the standard metal graphic procedure was used to polish the specimens. Finally, phase identification was performed by X-ray diffractometer (XRD, Bruker D8, Germany) with Cu Kα radiation. Microstructures and phase compositions were characterized by scanning electron microscope (SEM, Zeiss Merlin) coupled with energy-dispersive spectrometry (EDS).

2.3 Mechanical properties measurements

2.3.1 Tensile tests

Uniaxial quasi-static tensile tests were performed on the novel hybrid composite using a universal servo-hydraulic mechanical testing machine at room temperature in the open air. The dog-bone-shaped test specimens were machined from the composites using electro-discharge, and the gauge sections were 15 mm in length, 2.5 mm in width and 3 mm in thickness, as presented in Fig. 3a. Here, it should be noted that the volume ratio of the Ti-aluminide multi-layered part and the continuous-SiC_f-reinforced Ti-matrix part of the hybrid composite was processed to be 1:1. During the tensile test, the constant loading rate of the cross-head was set as 0.5 mm·min^{-1}, and the fracture surface morphology of the hybrid specimen was examined by SEM after tensile test.

2.3.2 Fracture tests

The hybrid composite was notched in different sides. For capturing and characterizing the cracks propagation during load process, all the tests were performed on a servo-
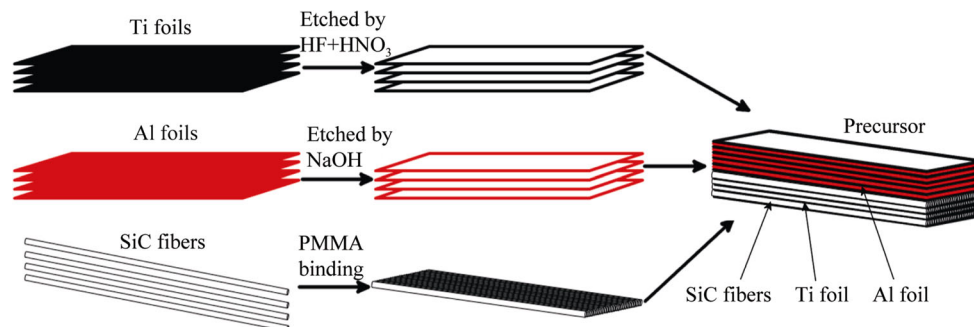

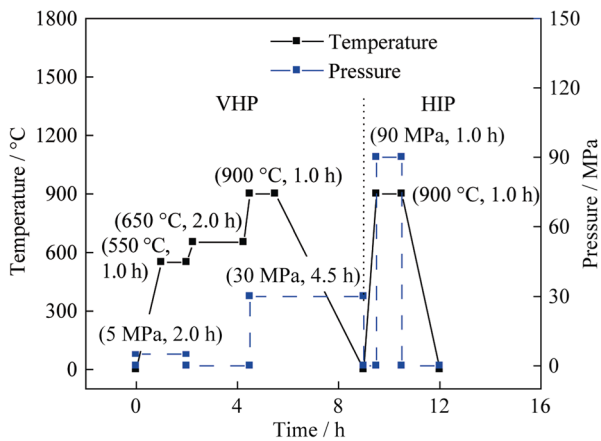**Fig. 1** Schematic illustration of fabrication process

Fig. 2 Fabrication parameters of hybrid composite

hydraulic loading system. This system was installed in the vacuum chamber of an SEM (Shimadzu Corporation, Japan) for obtaining an in situ observation. During the regular test, the constant loading rate was set as 0.1 mm·min^{-1}. The applied load value and displacement of the loading point can be simultaneously recorded during the test process, respectively. Noticeably, the test process would be frequently interrupted so as to record the in situ microcracks propagation morphologies. After each interruption, the test process would resume until the rupture of specimen. Figure 3b schematically illustrates the

dimensions and notched positions of the tested specimens, while the loading stage in the vacuum chamber of SEM is shown in Fig. 3c. Additionally, it should be mentioned that all the edge notch direction of the specimen is perpendicular to the layer direction, and this notch orientation style was also named crack arrester orientation in some other researches [19, 21]. Figure 3d,e represents the initial morphologies of the two types of notched specimens.

3 Results and discussion

3.1 SEM, EDS and XRD analyses of hybrid composite

The morphology of the prepared hybrid composite is shown in Fig. 4a. The Ti-aluminide multi-layered part and the continuous-SiC$_f$-reinforced Ti-matrix part are well integrated as a whole. In order to investigate the intermetallic layers and interfacial regions between the fibers and the Ti-matrix, backscattered electron (BSE) images coupled with line scan results of EDS are presented in Fig. 4b,c. Figure 4b indicates that there are several sublayers arranged from residual Ti layers to intermetallic layers. The variation in Ti and Al distributions detected by EDS line scan along the yellow line also confirms that Ti and Al foils react with each other during the sintering process. Meanwhile, EDS point analyses (marked by
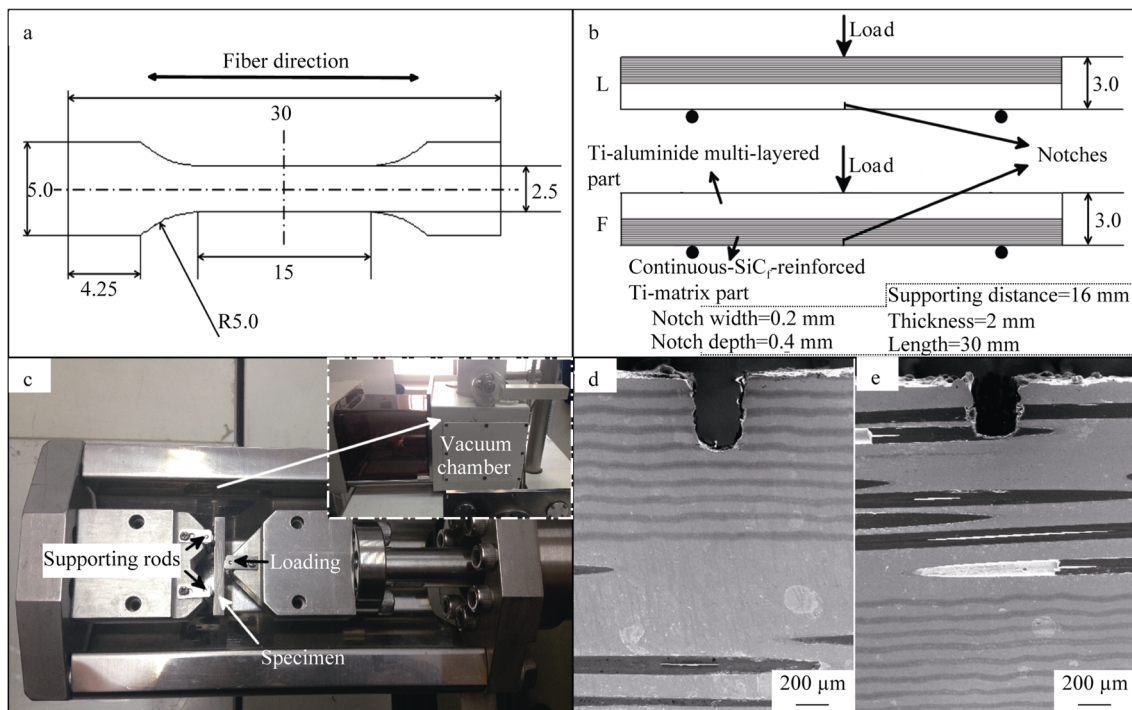

Fig. 3 Outline dimension of tensile test specimen (unit mm) a, schematic illustration of tested specimen in SEM in situ three-point bending test b, schematic diagram of the loading device inserted into SEM vacuum chamber c, SEM images of initial morphologies near notches of examined specimens: notched at Ti-aluminide multi-layered part d and notched at continuous-fiber-reinforced part e
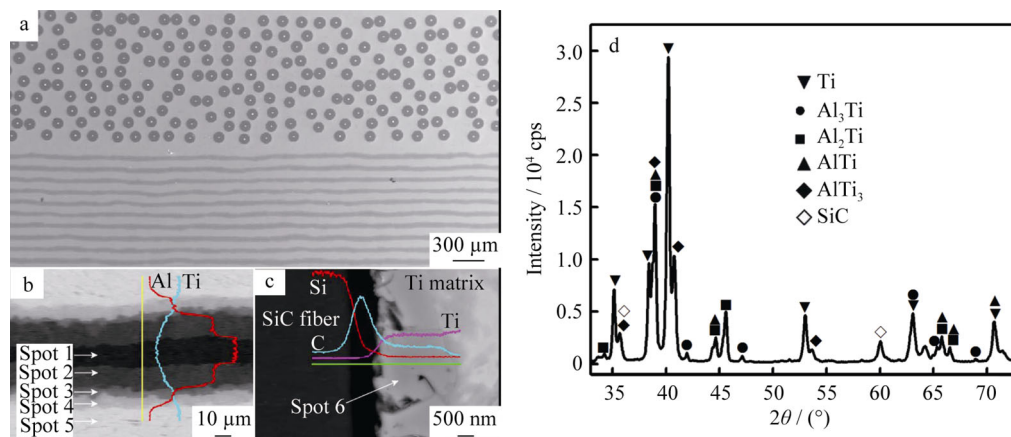
Fig. 4 Transverse SEM image of hybrid composite **a**, BSE images for EDS analysis of **b** Ti-aluminide part and **c** continuous-SiC$_f$-reinforced titanium part, and XRD pattern of hybrid composite **d**

arrows in Fig. 4b) were used for identifying the phases and the corresponding results are, respectively, shown in Table 1. Their chemical compositions are detected as Ti_3Al, $TiAl$, $TiAl_2$ and $TiAl_3$, which is consistent with the results in previous papers [21–23]. Additionally, by carefully scrutinizing the image (Fig. 4b), although the interfaces of the adjacent phases are wavy and not very straight at the microscale level, hardly any defects like holes and cavities can be found.

Figure 4c represents an area composed of two sublayers between SiC fiber and Ti-matrix. Herein, it can be inferred that the uniform dark layer surrounding SiC fiber is the carbon coating, and the other sublayer is the layer resulted from diffusive reaction between carbon coating and Ti-matrix. EDS line scan analysis was carried out along the green line (labeled in Fig. 4c) to investigate the distribution of Ti, Si and C elements within the interfacial region. EDS point detect was also performed to quantitatively clarify and characterize the phases within the interfacial region. In Fig. 4c, the results of EDS line scan analyses indicate that there exist apparent concentration gradients of Ti, Si and C elements along the green line, respectively. In particular, it can be found that Ti atoms diffuse from matrix toward to carbon coating so as to result in a decrease in concentration from the matrix to the carbon coating. On the other hand, C

Table 1 EDS results of marked points in Fig. 4 (at%)

Points	Ti	Al	C
Spot 1	25.03	74.97	–
Spot 2	35.22	64.78	–
Spot 3	49.76	50.24	–
Spot 4	71.98	28.02	–
Spot 5	99.31	0.69	–
Spot 6	48.43	–	51.57

atoms diffuse from carbon coating to Ti-matrix, which obviously demonstrates that carbon coating has already reacted with Ti-matrix during sintering process to form a gray reaction stripe as presented in Fig. 4c. And the result of EDS point detect (marked by arrow in Fig. 4c) indicates that the generated substance of gray stripe is TiC, and the corresponding results are also shown in Table 1. Noticeably, no trace of Si elements is found within the interfacial zone, which suggests that the carbon coating and generated TiC stripe isolate Ti-matrix and SiC fibers. In this way, SiC fibers are successfully protected [13, 24, 25]. Finally, XRD patterns in Fig. 4d validate the phase observation except TiC due to its low content.

3.2 Tensile properties and fracture surfaces of as-received hybrid composites

Typical strain and stress curves of the hybrid composite and Ti intermetallic multi-layered composite are shown in Fig. 5a. It can be seen that the ultimate tensile stress of hybrid composite is nearly about 545 MPa, which is higher than that of Ti intermetallic multi-layered composite (351 MPa) due to the introduction of the continuous-SiC$_f$-reinforced part. Figure 5b–d represents the morphologies of fracture surface of hybrid composite after tensile test. In Fig. 5b, fibers pullout in continuous-SiC$_f$-reinforced Ti-matrix part and the delamination in Ti-aluminide multi-layered part simultaneously occur during fracture. Specifically, as shown in Fig. 5c, dimples and tear ridges can be found in Ti-matrix of continuous-fiber-reinforced part. This indicates that the failure pattern of Ti-matrix material and SiC fibers is ductile brittle fracture, respectively [26, 27]. Furthermore, the detachment between SiC fiber and Ti-matrix indicates that the fiber stem has been detached from Ti-matrix along the surrounding reaction stripe and the

carbon-rich coating (labeled by arrow in Fig. 5c). In addition, most of the visibly reactive substance is still attached to Ti-matrix [28, 29]. Concerning the fractography of Ti-aluminide multi-layered part, rough fracture surface can be found in Fig. 5d, suggesting fracture mechanisms, such as the ductile fracture of Ti layers and brittle fracture of TiAl layers. Most important, some cracks (labeled by arrow in Fig. 5d) were terminated or blunted by Ti layers. This indicates that the ductile Ti layers can effectively suppress and prohibit the longitudinal propagation of cracks and restrict their spread within TiAl intermetallic layer.

3.3 Detailed fracture mechanisms by in situ mechanism

Typical load–displacement curves of specimens with different notched positions (notched at Ti-aluminide multi-layered part and notched at continuous-fiber-reinforced part, respectively) are shown in Fig. 6. The aslant discontinuous tails in the curves are resulted from several pauses when the in situ observations were conducted. From the distinct differences between those two curves, it can be deduced that the notched position is very important for the damage behavior of hybrid composite. For each curve, it can be divided into two sections. At the beginning, both

curves rapidly increase to their yielding points. However, after the yielding point, a higher and longer platform follows after one drop in the "L" curve, in comparison with the "F" curve. Although these two curves exhibit different patterns, their values are higher than that of Ti-aluminide multi-layered composite given by the red curve in Fig. 6. Therefore, it can be deduced that the mechanical properties
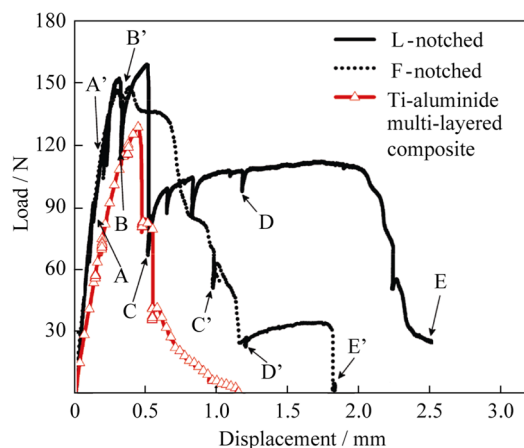

Fig. 6 Load–displacement curves of hybrid composite with different notch positions and Ti-aluminide multi-layered composite (letters being time when taking photographs corresponding to images in Figs. 7, 8)
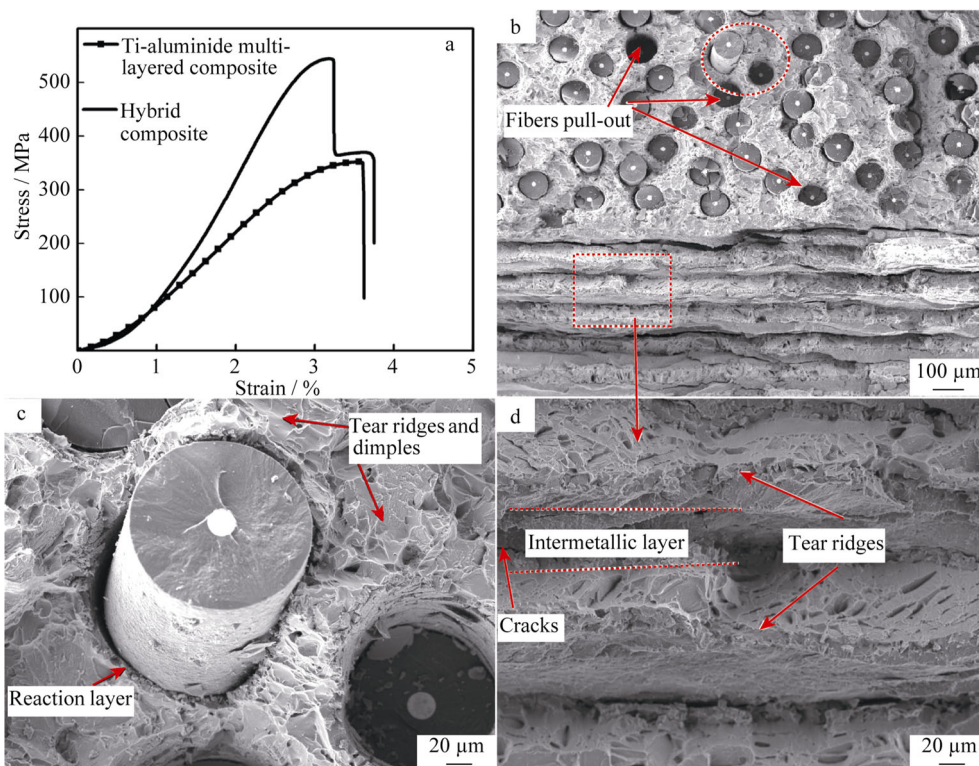

Fig. 5 Tensile stress–strain curves of hybrid composite (solid line) and Ti-aluminide multi-layered composite (neat composite) **a**; **b**, **c** and **d** are fractographs of hybrid composite after tensile test
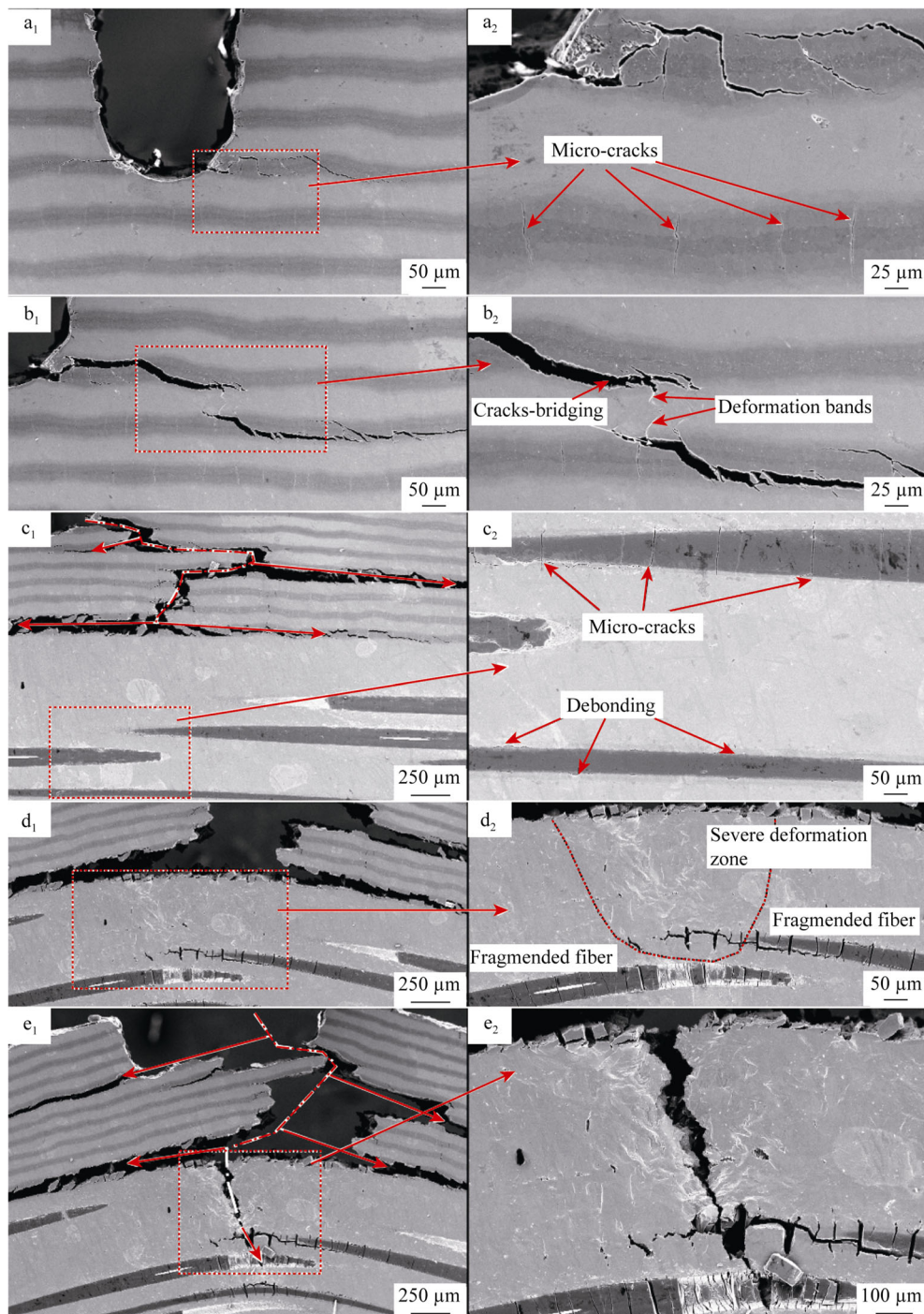
Fig. 7 SEM images for crack propagation process where notch position is located at Ti-aluminide multi-layered part during in situ three-point bending test: a_1–e_1 main crack propagation process at different loading stages and a_2–e_2 highly amplified SEM images of localized regions of cracks

of the novel hybrid composite are enhanced by the introduction of the continuous-SiC$_f$-reinforced Ti-matrix part.

Figure 7 represents progressive deformation process of the L-notched sample during bending test. At the beginning of the load, corresponding to the Point A in the solid line

curve in Fig. 6, a few cracks generate and circuitously propagate along brittle aluminide layer. In addition to these mesoscale cracks, some tiny cracks (marked by the arrows in Fig. 7a$_2$) can also be found. In contrast with the orientation of these mesoscale cracks, the primarily propagative
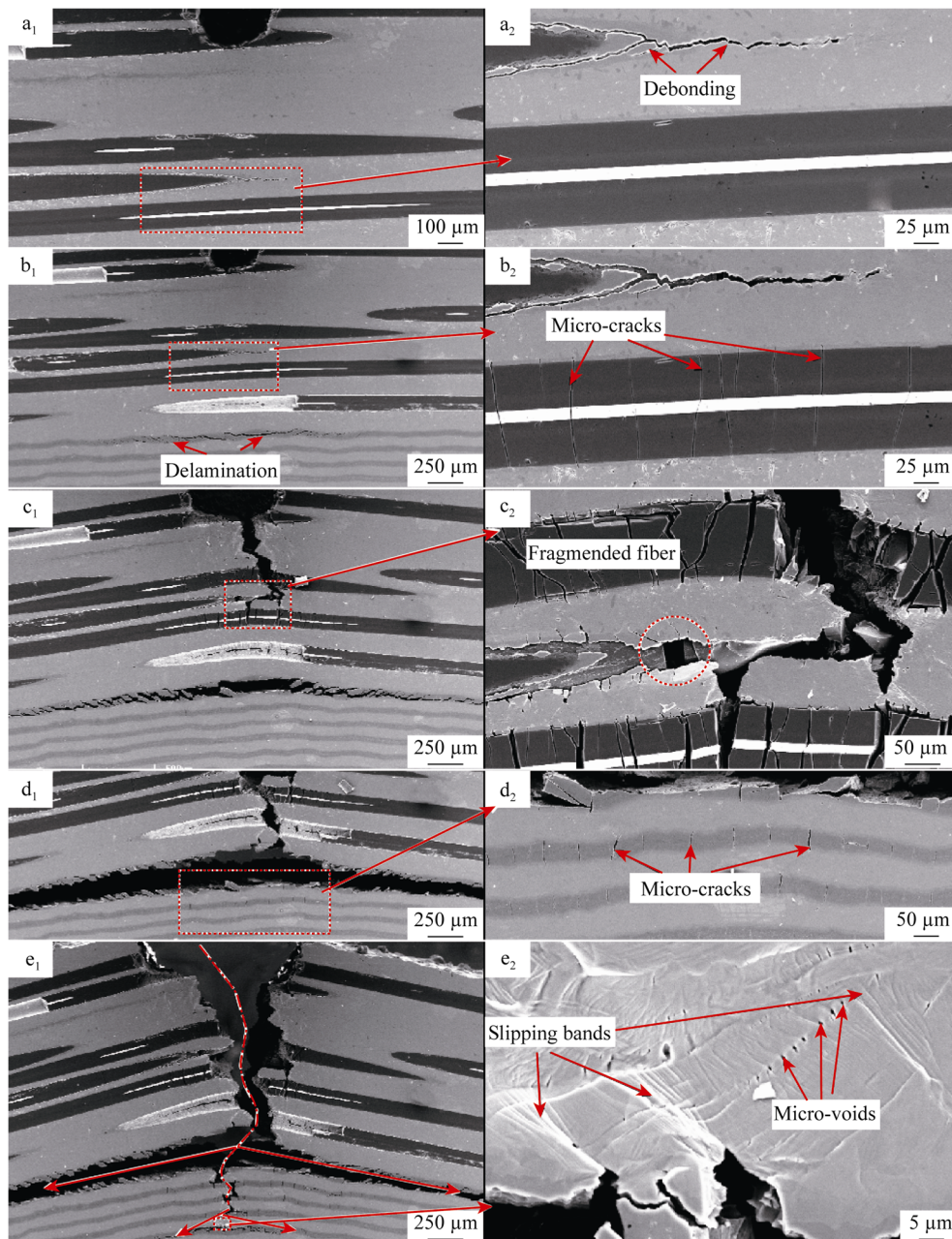
Fig. 8 SEM images for crack propagation process where notch position is located at continuous-SiC$_f$-reinforced Ti-matrix part during in situ three-point bending test: a_1–e_1 main crack propagation process at different loading stages and a_2–e_2 highly amplified SEM images of localized regions of cracks

orientations of the tiny cracks are mainly perpendicular to the adjacent ductile layers. However, no crack is found within ductile Ti layers at this moment. With the load increasing, as shown in Fig. 7b$_1$, the previously formed cracks continuously extend within intermetallic layers along the horizontal direction. Continuously, some cracks (marked by arrows in Fig. 7b$_2$) pass through contiguous Ti layers from one intermetallic layer to another due to the crack bridging mechanism of ductile Ti layers. Although

the further magnification of this area demonstrates that plastic deformation occurs within Ti layers, no crack is found. After that, as shown in Fig. 7c$_1$, a mess of cracks generate and propagate in many intermetallic layers, while the residual Ti layers present severely plastic deformation to induce its strain strengthening. Therefore, based on the aforementioned characteristics, it can be deduced that Ti intermetallic multilayers have an important role to deflect, blunt and bridge the propagation of the cracks. With the

load increasing, the cracks start to penetrate into continuous-fiber-reinforced part. Although several fibers have already been fractured (marked by arrows in Fig. 7c$_2$), none of cracks are found in Ti-matrix. After that, the cracks continuously and simultaneously propagate toward to Ti-matrix and fiber matrix, respectively. As mentioned in some previous studies [30, 31], the carbon coating surfaces of the SiC fibers have been already roughed and corroded due to the interfacial diffusive reactions, which is detrimental to the mechanical properties of SiC fibers. However, in comparison with fragile SiC fibers under the external load, the ductile Ti-matrix exhibits the opposite characteristic. All of the initial cracks originated from TiC bands are suppressed by the plastic deformation zone in Ti-matrix (labeled by dotted line in Fig. 7d$_2$). Finally, the sample is ruptured after experiencing a long elastic/plastic deformation stage, as shown in Fig. 7e$_1$, e$_2$. Based on above discussion, the extrinsic toughening mechanisms, such as crack deflection, crack bridging and crack blunt, unitedly have important roles in extending the length of crack propagation paths. Finally, these enhance the whole mechanical properties of this hybrid composite.

Figure 8 represents similar deformation process of F-notched specimen during bending test. Firstly, debonding (marked by arrows in Fig. 8a$_2$) happens between the fibers, which is corresponding to Point A' in dotted curve shown in Fig. 6. Subsequently, the fibers (marked by arrows in Fig. 8b$_2$) are bent to be fragmented due to the same reason discussed in above paragraph. Noticeably, the whole surface of hybrid composite indicates that the delamination (marked by arrows in Fig. 8b$_1$) also occurs in Ti-aluminide multi-layered part at this moment, which is different from the deformation process of L-notched specimen. It can be inferred that microcracks have already been generated in intermetallic layers due to localized higher stress concentration resulted from its coordinative deformation behavior, and the consecutive Ti-matrix of the continuous-fiber-reinforced part is progressively torn to be ruptured. Ultimately, the cracks progressively penetrate into Ti-aluminide multi-layered part and cause the failure of the specimen. Noticeably, premature cracks originated in Ti-aluminide multi-layered part give rise to detrimental effect on mechanical properties of F-notched specimen.

4 Conclusion

In this study, a composite composed of Ti-aluminide multi-layers and continuous-SiC$_f$-reinforced Ti-matrix was successfully fabricated using VHP/HIP sintering process through pure Ti foils, pure Al foils and continuous SiC fibers. Microstructural observations reveal that all of Al foils were consumed into forming a series of intermetallic phases.

Meanwhile, a thin (1 μm in thickness) circle TiC stripe forms between Ti-matrix and carbon coating deposited on SiC fiber. Owing to the incorporation of the continuous-SiC$_f$-reinforced Ti-matrix part, the tensile strength (545 MPa) of the hybrid composite is much higher than that of neat multi-layered composite (351 MPa). Furthermore, in situ observations reveal that extrinsic toughening mechanisms are the key reasons of the excellent damage tolerance, which contains crack deflection, crack blunt and crack bridging. In particular, when the notch position is located in the Ti-aluminide multi-layered part (L-notched sample), the better damage tolerance behavior is presented.

References

[1] Guo YJ, Shi ZQ, Xu YK, Qiao GJ. Correlation between microstructure and tensile behavior of metal–intermetallic laminate compound with different initial Ni foil thickness. Rare Met. 2014;33(2):196.

[2] Shen Z-Z, Lin J-P, Liang Y-F, Zhang L-Q, Hao G-J. Reaction behaviors occurring in Ti/Al foil metallurgy. Rare Met. 2015;35(1):100.

[3] Wang Y, Vecchio KS. Microstructure evolution in Fe-based-aluminide metallic–intermetallic laminate (MIL) composites. Mater Sci Eng A. 2016;649(1):325.

[4] Kim IK, Hong SI. Mechanochemical joining in cold roll-cladding of tri-layered Cu/Al/Cu composite and the interface cracking behavior. Mater Des. 2014;57(5):625.

[5] Rawers JC, Alman DE. Fracture characteristics of metal/intermetallic laminar composites produced by reaction sintering and hot-pressing. Compos Sci Technol. 1995;54(4):379.

[6] Alman DE, Rawers JC, Hawk JA. Microstructural and failure characteristics of metal-intermetallic layered sheet composites. Metall Mater Trans A. 1995;26(3):589.

[7] Adharapurapu RR, Vecchio KS, Jiang FC, Rohatgi A. Effects of ductile laminate thickness, volume fraction, and orientation on fatigue-crack propagation in Ti–Al$_3$Ti metal-intermetallic laminate composites. Metall Mater Trans A. 2005;36A(6):1595.

[8] Adharapurapu RR, Vecchio KS, Rohatgi A, Jiang FC. Fracture of Ti–Al$_3$Ti metal-intermetallic laminate composites: effects of lamination on resistance-curve behavior. Metall Mater Trans A. 2005;36A(11):3217.

[9] Yu W, Zhu K, Aman Y, Guo Z, Xiong S. Bio-inspired design of SiC$_f$-reinforced multi-layered Ti-intermetallic composite. Mater Des. 2016;101(7):102.

[10] Rohatgi A, Harach DJ, Vecchio KS, Harvey KP. Resistance-curve and fracture behavior of Ti–Al$_3$Ti metallic–intermetallic laminate (MIL) composites. Acta Mater. 2003;51(10):2933.

[11] Li T, Jiang F, Olevsky EA, Vecchio KS, Meyers MA. Damage evolution in Ti6Al4V–Al$_3$Ti metal-intermetallic laminate composites. Mater Sci Eng A. 2007;443(1–2):1.

[12] Froes FH, Suryanarayana C, Eliezer D. Synthesis, properties and applications of titanium aluminides. J Mater Sci. 1992;27(19):5113.

[13] Zhang W, Yang YQ, Zhao GM, Feng ZQ, Huang B, Luo X, Li MH, Chen YX. Interfacial reaction studies of B$_4$C-coated and C-coated SiC fiber reinforced Ti–43Al–9V composites. Intermetallics. 2014;50(4):14.

[14] Fu YC, Shi NL, Zhang DZ, Yang R. Effect of C coating on the interfacial microstructure and properties of SiC fiber-reinforced Ti matrix composites. Mater Sci Eng A. 2006;426(1–2):278.

[15] Jeng SM, Yang JM, Rosenthal DG, Aksoy S. Mechanical behaviour of SiC fibre-reinforced titanium/titanium aluminide hybrid composites. J Mater Sci. 1992;27(19):5357.

[16] Lou JH, Yang YQ, Sun Q, Li J, Luo X. Study on longitudinal tensile properties of SiC$_f$/Ti–6Al–4V composites with different interfacial shear strength. Mater Sci Eng A. 2011;529(1):88.

[17] Naseem K, Yang Y, Luo X, Huang B, Feng G. SEM in situ study on the mechanical behaviour of SiC$_f$/Ti composite subjected to axial tensile load. Mater Sci Eng A. 2011;528(13–14):4507.

[18] Luo X, Yang Y, Sun Q, Yu Y, Huang B, Chen Y. Effect of Cu/Mo duplex coating on the interface and property of SiC$_f$/Ti6Al4V composite. Mater Sci Eng A. 2012;535(4):6.

[19] Oh J, Lee WC, Pyo SG, Park W, Lee S, Kim NJ. Microstructural analysis of multilayered titanium aluminide sheets fabricated by hot rolling and heat treatment. Metall Mater Trans A. 2002;33(12):3649.

[20] Kai Z, Yu W, Yann A, Tao J. Synthesis, microstructure and mechanical properties of a bio-inspired Ti-intermetallic multi-layered/SiC$_f$-reinforced Ti-matrix hybrid composite. J Mater Sci. 2016;51(18):8747.

[21] Sun Y, Haley J, Kulkarni K, Aindow M, Lavernia EJ. Influence of electric current on microstructure evolution in Ti/Al and Ti/TiAl$_3$ during spark plasma sintering. J Alloys Compds. 2015;648(13):1097.

[22] Loo FJJv. Diffusion in the Titanium–Aluminium System. Eindhoven: Technische Hogeschool Eindhoven; 1971. 58.

[23] van Loo FJJ, Rieck GD. Diffusion in the titanium-aluminium system—I. Interdiffusion between solid Al and Ti or Ti–Al alloys. Acta Metall. 1973;21(1):61.

[24] Djanarthany S, Viala J-C, Bouix J. Development of SiC/TiAl composites: processing and interfacial phenomena. Mater Sci Eng A. 2001;300(1–2):211.

[25] Tesha JV, Stephenson DJ, Hancock P. A new criterion for determining the failure of Ti/SiC metal-matrix composites. J Mater Sci. 1994;29(22):5787.

[26] Luo X, Yang Y, Yu Y, Wang X, Huang \hen Y. Effect of Mo coating on the interface and mechanical properties of SiC fiber reinforced Ti6Al4V composites. Mater Sci Eng A. 2012;550(6):286.

[27] Guo S. Improvement of mechanical properties of SiC(SCS-6) fibre-reinforced Ti$_3$AlC$_2$ matrix composites with Ti barrier layer. J Eur Ceram Soc. 2016;36(6):1349.

[28] Ward-Close CM, Partridge PG. A fibre coating process for advanced metal-matrix composites. J Mater Sci. 1990;25(10):4315.

[29] Jeng SM, Yang JM, Rosenthal DG, Aksoy S. Mechanical behaviour of SiC fibre-reinforced titanium/titanium aluminide hybrid composites. J Mater Sci. 1992;27(19):5357.

[30] Xiao Z, Yang Y, Luo X, Huang B. Investigation of interfacial reaction product of SiC$_f$/C/Mo/Ti6Al4V composite through Raman spectroscopy. Appl Phys Lett. 2014;104(8):081611.

[31] Luo X, Yang Y, Li J, Mei Y, Yuan M, Chen Y. The effect of fabrication processes on the mechanical and interfacial properties of SiC$_f$/Cu–matrix composites. Compos A. 2007;38(10):2102.